water

MDPI

Article

Real-Time Properties of Hydraulic Jump off a Tidal Bore, Its Generation and Transport Mechanisms: A Case Study of the Kampar River Estuary, Indonesia

Ulung Jantama Wisha [1,2,3], Yusuf Jati Wijaya [1,4] and Yukiharu Hisaki [1,*]

[1] Physical Oceanography Laboratory, Department of Physics and Earth Sciences, Graduate School of Engineering and Science, University of the Ryukyus, Nishihara-cho 903-0213, Japan
[2] Research Institute for Coastal Resources and Vulnerability, Ministry of Marine Affairs and Fisheries, Padang 5245, Indonesia
[3] Research Center for Oceanography, National Research and Innovation Agency, Jakarta 14430, Indonesia
[4] Department of Oceanography, Faculty of Fisheries and Marine Science, Diponegoro University, Semarang 50275, Indonesia
* Correspondence: hisaki@sci.u-ryukyu.ac.jp

Abstract: Since the hydraulic jump off a tidal bore in the Kampar Estuary has never been well-described, real-time measurements of hydraulic jump properties are crucial to understanding the tidal bore characteristics. This study aims to determine the real-time properties of a tidal bore generation, hydraulic jump, and transport mechanism in the Kampar River estuary. Tidal harmonic and range are analyzed using least-square-based tidal modeling. The tidal bore height and turbulent velocity records based on ADCP surveys in the estuary and upstream area are used to determine the hydraulic jump properties. Furthermore, an acoustic-based approach is also employed to quantify the suspended sediment concentration and flux during the passage of the bore. Kampar Estuary is predominated by semidiurnal co-tidal components (M2 and S2), where, based on the phase lag magnitude, it is categorized as an ebb-dominant estuary. This finding is proven by the more intense and prolonged ebb phases, especially during spring tidal conditions where the tidal range reaches 4 m. Of particular concern, the tidal bore height declines by 1.5 m every 20 km upstream with an erratic turbulent velocity. A sudden increase in transverse and vertical velocity during the passage of bore (ranging from −0.9 to 0.2 m/s) reflects the potency of sediment resuspension in the surrounding river edge marked by the significant increase in suspended sediment flux of about 3.7 times larger than at the end of the ebb tide. However, long-term measurement and regular bathymetry surveys are crucial to monitor the tidal bore behavior and morpho-dynamics in the Kampar River estuary.

Keywords: turbulent velocity; transport mechanism; tidal range; suspended sediment flux

Citation: Wisha, U.J.; Wijaya, Y.J.; Hisaki, Y. Real-Time Properties of Hydraulic Jump off a Tidal Bore, Its Generation and Transport Mechanisms: A Case Study of the Kampar River Estuary, Indonesia. *Water* **2022**, *14*, 2561. https://doi.org/10.3390/w14162561

Academic Editor: Mouldi Ben Meftah

Received: 6 July 2022
Accepted: 18 August 2022
Published: 19 August 2022

1. Introduction

An estuary is a significant and unique water area where oceanographic and anthropogenic factors shape its characteristics [1], impacting the river and estuary's physical, biological, geological, and even chemical states [2]. As the place of sea-river water confluence, tidal influence is considerable in estuaries, playing a significant role in controlling transport mechanisms in the form of oscillations in the estuary [3]. These tidal oscillations are associated with large mixing within estuarine water [4], transporting and scouring bed sediment along the river [5]. These large transports can result in tidal bore propagation often seen in estuarine waters.

A tidal bore is a tidal wave commonly observed in estuarine waters generated by a relatively high tidal range and large river streams, surging upstream because of different hydraulic pressure [1,2,6,7]. According to [8], a tidal bore is an unsteady water movement induced by a rapid surface water-level rise at the mouth of the estuary during the early

high tidal phase. With time, the first wave crest becomes steeper and steeper until it forms a wall of water propagating upstream. The first wave crest is characterized by the train of a secondary wave following the non-breaking surge front [1,9]. According to [10], the hydraulic jump off the tidal bore induces scouring and turbulence beneath the first wave crest. Therefore, revealing the real-time hydraulic jump properties is essential in determining the process and evolution of bore-affected estuaries.

It is estimated that there are more than 400 bore-affected estuaries worldwide [1,11]. There are about five tidal bore symptoms scattered throughout the Indonesia archipelago. However, tidal bore records and studies are relatively limited due to the difficult access to sites. By contrast, a tidal bore in the Kampar Estuary is the most well known and frequently studied, precisely located in the Pelalawan Regency, Riau Province, Indonesia (Figure 1). This tidal bore, called Bono, was scientifically reported for the first time by [12], who conducted a qualitative survey and modeled the symptoms of abrasion and accretion in the estuary of the Kampar River. The Kampar River estuary is a macro-tidal estuary with a funnel shape (V-shape) whereby the river width and depth gradually decline upstream [4]. In subsequent studies, [13] surveyed one-line parallel bathymetry data along the Kampar River, reporting that the tidal bore propagates upstream, reaching 60 km from the estuary. On the other hand, local researchers and scholars have conducted several environmental-based studies in the Kampar Estuary [14–18].

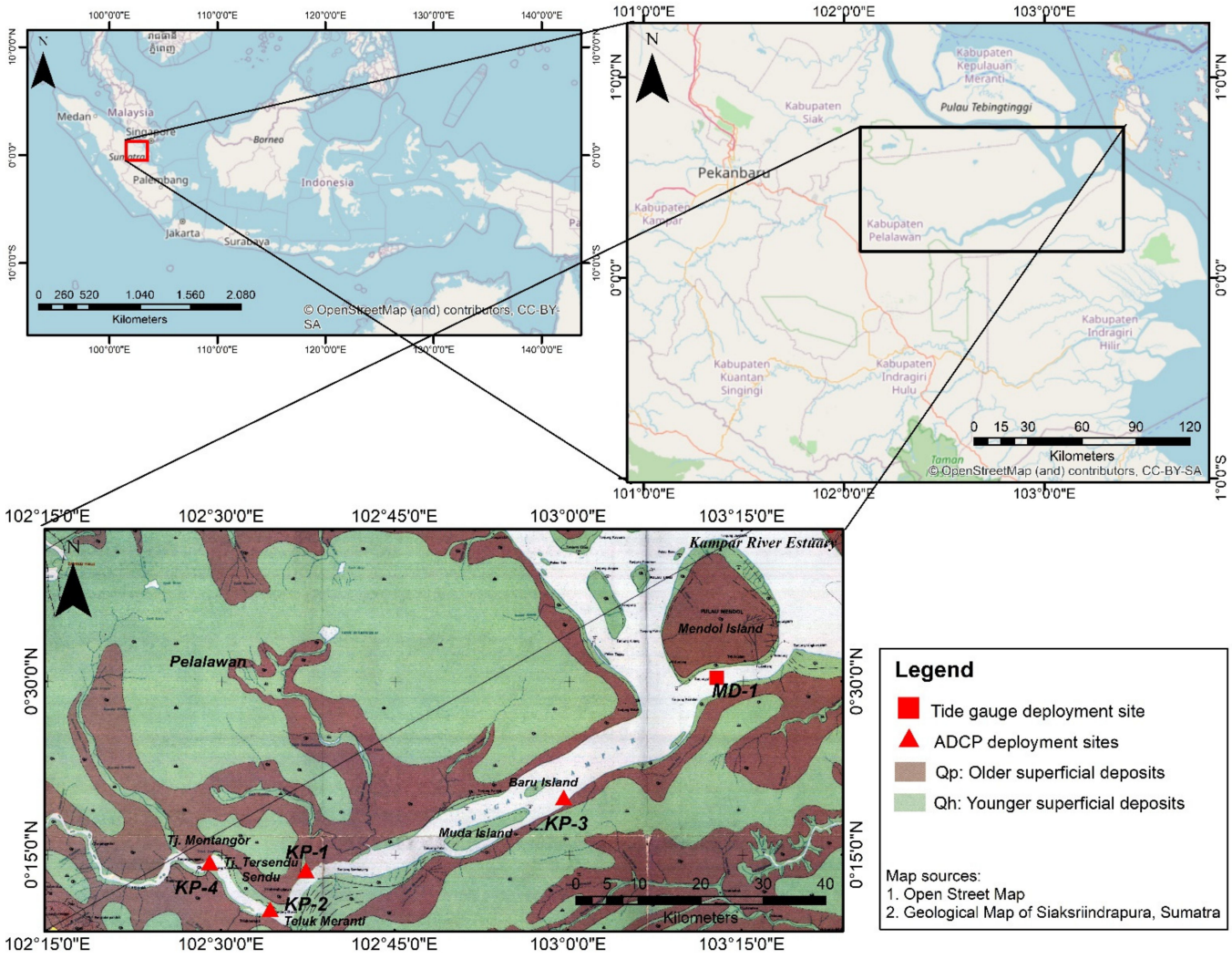

Figure 1. Details of the Kampar River estuary and observation sites.

Numerous numerical hydraulic jump models in the Kampar River have also been developed [3,19–21]. Overall, numerical model approaches employed by previous studies have never been well validated using field data measurements or calibrated using local bathymetry. Even though some reports explicitly mentioned the hydraulic jump records in the Kampar Estuary [4,17], these data did not describe the properties of a tidal bore well. Since the established data of tidal bore motions in the Kampar Estuary are limited, the hydraulic jump properties of the tidal bore are crucial to determine. Moreover, to date, the turbulent velocity regimes during the passage of bores in the Kampar Estuary are not yet clearly explained. As previously reported by [5,10,22–25], a rapid increase in water level (hydraulic jump) is characterized by a sharp rise in turbulent velocity, playing a role in the transport mechanism throughout the river. Therefore, we report herein the record of hydraulic jump and turbulent velocities off a tidal bore in the Kampar River estuary, based on the ADCP (Acoustic Doppler Current Profiler) survey deployed simultaneously in several significant areas along the river. A few studies have reported the influence of the passage of bores on suspended sediment fluctuation [26,27], and this is one aspect that should be investigated. Therefore, this study aims to determine the real-time tidal bore generation, hydraulic jump properties, and transport mechanism in the Kampar River estuary.

2. Materials and Methods

2.1. Study Site and Field Observation

The study area is situated in the Kampar River estuary, Pelalawan Regency, Riau Province, Indonesia, categorized as a river watershed area geographically positioned at 0°40′0″–0°13′20″ north and 102°40′0″–103°26′40″ east (Figure 1). Geologically, Kampar River lies between two rock formations; younger superficial deposits (Qh) composed of clay, silt, gravel, plant waste, peat swamp, and coral reefs; and older superficial deposits (Qp) composed of clay, silt, sandy clay, plant waste, and sandy granite (Figure 1) [4].

Kampar River is the largest river in Riau Province, with an approximate length of 400 km from the estuary to upstream, sourced from Bukit Barisan mountains, passing through several regencies (Indragiri Hulu, Indragiri Hilir, Kampar, Kuantan Singing, Pelalawan, Siak, and Pekanbaru), and eventually ending up in the Malacca Strait. Moreover, the area of Kampar River reaches 24,548 km^2 with a river discharge of approximately 600 m^3/s upstream and 200 to 400 m^3/s downstream [28].

Kampar River is a shallow downstream river with a funnel (V-shaped) formation. In several areas close to the estuary, enormous abrasions have frequently occurred, and unstable sediment transport is highly controlled by a destructive tidal bore phenomenon called Bono [12].

Field surveys were conducted twice (April and August 2016) by the Research Institute for Coastal Resources and Vulnerability, Ministry of Marine Affairs and Fisheries, Indonesia. A simultaneous ADCP (Acoustic Doppler Current Profiler) deployment was carried out throughout the Kampar River estuary (Nortek^{TM} Aquadopp Profiler 600 kHz and Teledyne RDI Workhorse ADCP). Due to safety reasons, the instruments were deployed no longer than 48 h. The instrument setup and specifications are shown in Table 1. Moreover, except for station KP-4, the data yielded from the ADCP surveys consisted of surface elevation changes, turbulent velocity profiles, and water temperature.

On the other hand, to understand the tidal-generated bores in the estuary, a Tide Master Valeport vented strain gauge was deployed for 38 days from 23 April to 31 May 2016, mounted close to Mendol Island (Figure 1). The filtered tidal data were then analyzed to gain harmonic tidal constituents and tidal range profiles, which will be elucidated in Section 2.3.

Table 1. Details of deployment setup and instrument specifications.

Observation Station	Area Location	Deployment Coordinates		Instrument Specifications	Deployment Setup	Survey Period (Western Indonesian Time UTC+07:00)
		Longitude	Latitude			
MD-1	Mendol Island	103.212° E	0.503° N	**Tide Master Valeport** Range: min 0.8 m and max 20 m Beam angle: ± 6° Frequency: 25 GHz Accuracy: ± 10 mm Precision: 1 mm	• Mode: B4 • Pressure units: meter • User pressure cal: Gain 1.026967, Offset −0.011763 • Vale pressure cal: P0 = 2.49 × 10^{-9}E-09, P1 = 0.003178, P3 = −1.880864 • Calibrated: 12 November 2015	23 April 2016 15:45 to 31 May 2016 16:00
KP-1	Tanjung Tersendu-sendu	102.624° E	0.225° N	**ADCP Nortek Aquadopp** Acoustic frequency: 0.6 MHz Max profile range: 30–40 m Cell-size: 1–4 m Minimum blanking: 0.5 m Max cell: 128 Velocity range: ± 10 m/s Accuracy: 1% of measured value ± 0.5 m/s Max sampling range: 1 Hz	• Profile interval: 300 s • Number of cell sizes: 8 • Cell size: 1 m • Blanking distance: 0.5 m • Measurement load: 100% • Average interval: 60 s • Compass update range: 300 s	24 April 2016 13:30 to 25 April 2016 14:55
KP-2	Teluk Meranti	102.568° E	0.165° N			25 April 2016 17:00 to 26 April 2016 17:25
KP-3	Baru Island	103.005° E	0.336° N			20 August 2016 11:00 to 22 August 2016 19:55
KP-4	Tanjung Mentangor	102.480° E	0.241° N	**Teledyne RD Instrument Workhorse Sentinel** Center working frequency: 614 kHz Max. typical profiling range: 70 m Nadir angle: 20 deg Max. number of cells per beam: 256 Min. Blanking distance: 0.5 m Cell size: 0.25–4 m Max. ping range: 3 Hz Max. velocity: 10 m/s Cell overlap: 25%	• Ensemble interval: 300 s • Frequency: 614.4 kHz • Beam angle: 20 deg • Deployment hours: 120 • Pings/Ens: 50 • Time/ping: 6 min • First cell range: 2.11 m • Cell size: 1 m	21 August 2016 11:30 to 23 August 2016 15:00

2.2. Mounting Scheme and Geometry of Kampar River

Based on national bathymetric data calibrated using a single beam echosounder measurement, the bathymetry profile of the Kampar River estuary varies considerably. It ranges from 2.3 to 6.2 m in the surrounding mouth of the estuary. It becomes significantly shallow in the surrounding Muda Island (wave energy mixing zone) [4] with a water depth ranging from 0.1 to 1 m, and it gradually gets a little bit deeper after passing Tanjung Tersendu-sendu area (station KP-1), ranging from 0.6 to 2.5 m (Figure 2A). Several sandbank formations are observed in the Tanjung Mentangor area, where the tidal bore is reported to be decaying at this point.

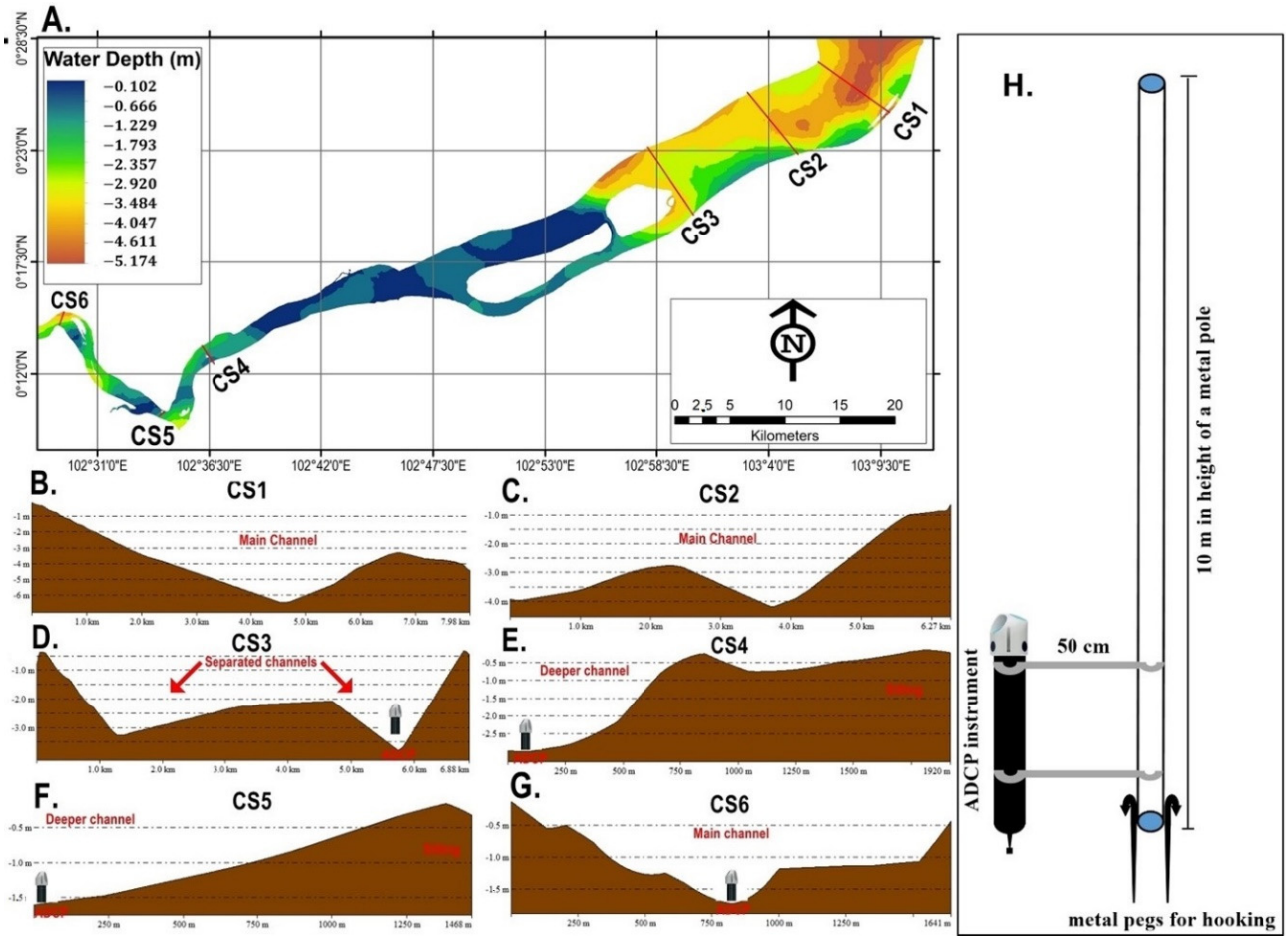

Figure 2. Bathymetry and geometry profiles of the Kampar River estuary calibrated using a field survey in 2016 (**A**); cross-section in the mouth of the estuary (**B**); cross-section in the main channel shifting (**C**); cross-section in separated channels in front of Baru Island with an ADCP deployment scheme (Station KP-3) (**D**); cross-section in the remnant observation stations (**E**–**G**); mounting scheme of ADCP instruments (**H**). Dotted lines denote the bathymetry (depth level) in every cross-section.

Based on the cross-section of the bottom morphology (Figure 2B–G), the Kampar River estuary has a funnel-shaped formation (V-shape) where the river width declines upstream, ranging from 1 to 8 km from upstream to downstream. Because of the unstable bore-induced sedimentation, the bathymetry of the river (and mouth) often changes, resulting in complex hydrodynamic systems that regularly alter the position of the Kampar River's main channel. Passing through Baru and Muda Island, located right in the middle of the river, the channel is separated, and the depth decreases considerably, with a magnitude of approximately 4 m. Shoaling effects in this super shallow area are possible because of the significant bathymetry changes, inducing a greater propagation of bores and local erosion [4,17,29]. The bores coalesce after passing Muda Island, forming higher waves [12].

The processes that occur during the passage of bores are presumed to induce a varied bottom sediment transport and resuspension.

Referring to [4], mixed-sediment types have been observed in the mouth of the estuary (clayey silt, silt, and sandy silt) and the area of tidal bore decay (sand, silty sand, sandy silt, and silt). In contrast, sand sediment is predominated in the middle of the river, where mixed wave energy occurs. Therefore, sand sediment settling in the area around Muda Island creates a super rigid bottom substrate. This state also becomes a reason why a mounting scheme of ADCP could not be performed throughout this area.

Concerning the ADCPs, they were deployed in the area with a depth of more than one meter, attached to a metal pole to maintain the position of the instruments. The first deployment was situated at stations KP-1 and KP-2, representing the middle river zone. The second measurement was positioned at stations KP-3 and KP-4, representing the downstream and upstream areas (Figure 2B–G), respectively. The mounting scheme of ADCPs applied in the field is shown in Figure 2H, where using a 10 m metal pole was possible to maintain the position of the ADCP. The pole was hooked using several metal pegs in the bottom part. The instrument's distance from the pole was 50 cm, attached by other more minor metals connected to the central pole.

2.3. Tidal Data Analyses

Since tidal data measurement in August 2016 could not be performed due to technical reasons, we employed a month's tidal prediction data provided by the Geospatial Information Agency of Indonesia (BIG), retrieved from a webpage: https://srgi.big.go.id/tides, accessed on 12 May 2022. We collected the data at a coordinate of 103.2075° E and 0.5143° N, right at station MD-1 (Figure 1).

The collected tidal data were modeled for 18.6 years using a NAO.99b program developed by National Astronomical Observatory, Tokyo, Japan [30]. All the data were then filtered to be analyzed using the ERG program, a program developed by Bandung Institute of Technology, Bandung, Indonesia, consisting of three primary sub-programs: ERGRAM, ERGELV, and ERGTIDE [31]. These programs are developed based on a least-square method [32]. The significant elevation-dependent mean sea level and harmonic constituents were obtained from this simulation.

As previously reported by several scholars [3,33–35], in the study area, the semidiurnal components (M2 and S2) are predominant. Therefore, because the influence of diurnal components is extremely low on shaping the tidal asymmetry [36], we focused on the two most significant semidiurnal constituents to be analyzed in more detail. The tidal model was equipped with an online Fourier analysis, quantitatively estimating the co-tidal constituent distribution across the study area. The co-tidal charts were then interpolated using spline interpolation to minimize the total surface curvature [37].

Aside from harmonic analysis, the field-measured and predicted tidal data were also filtered according to the moon phase. As an astronomically influenced oceanographic parameter, the surface elevation and the tidal forcing vary depending on the position of the moon, the earth, and the sun [38,39]. The following stage involved quantifying the tidal range and the displacement period of sinusoidal tides by subtracting the top and trough elevation data starting from the slack after flood tides up to the ebb slack point during neap and spring phases [40]. Furthermore, the displacement period for one cycle of tides was calculated using the record of tidal modulations as follows:

$$TR = \left| \zeta_{high\ tide} - \zeta_{low\ tide} \right| \quad (1)$$

$$DP = \left| t_{high\ tide} - t_{low\ tide} \right| \quad (2)$$

where:

TR = tidal range

ζ = tidal elevation (m)

DP = displacement period
t = time (hours)

2.4. Calculating the Approximate Tidal Bore Height

A previous study conducted by the authors in another site (Rokan Estuary) elucidated the same workflow concerning tidal data analyses and tidal bore height calculation [25]. The tidal bore front features could be approached from a quasi-steady flow analogy with tidal bore celerity U (Figure 3), considering mass and momentum conservation [1,26] as follows:

$$(V_1 + U)wl_1 = (V_2 + U)wl_2 \tag{3}$$

$$\frac{1}{2}\rho g\left(wl_2^2 - wl_1^2\right) = \rho(V_1 + U)wl_1(V_1 - V_2) \tag{4}$$

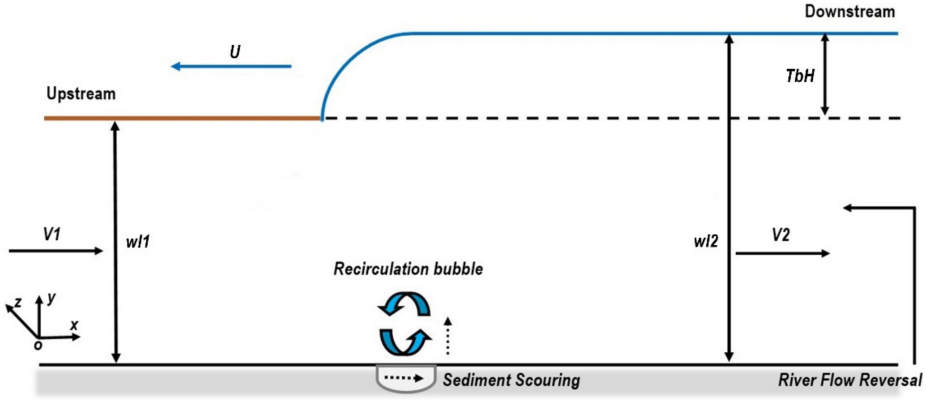

Figure 3. Definition sketch of a quasi-steady flow of tidal bores, modified from [22]. The blue line shows the tidal bore surface flow, and the brown line shows the initial water level before the tidal bore passage. Horizontal arrows denote the main water flow direction.

According to [22], Equations (3) and (4) are valid for stationary hydraulic jumps ($U = 0$), the tidal bore passage ($U > 0$), and positive surges flowing downstream ($U < 0$). Then, the solution to Equations (3) and (4) results in the height of the tidal bore Tb_H and Froude number Fr as follows:

$$Tb_H = \frac{wl_1}{2}\left(\sqrt{1 + 8Fr^2} - 3\right) \tag{5}$$

$$Fr = \frac{V_1 + C}{\sqrt{gwl_1}} \tag{6}$$

$$Tb_H = wl_2 - wl_1 \tag{7}$$

where:
U = tidal bore celerity measured in the field positive upstream (m/s)
V_1 = initial cross-sectional average flow velocity (m/s)
V_2 = cross-sectional average flow velocity after the bores propagate (m/s)
wl_1 = initial water level (m)
wl_2 = water level after the bores propagate (m)
ρ = water density (kg/m^3)
g = acceleration of gravity (9.81 m/s^2)
Tb_H = tidal bore height (m)
Fr = Froude number

2.5. Acoustic-Based Suspended Sediment Estimation

Aside from tidal bore and velocity measurements, the strength of reverberated sound was analyzed to determine the relationship between the relative acoustic backscatter (RB) and estimated SSC (suspended sediment concentration) [41–43] as follows:

$$SSC = 10^{(A+B.RB)} \quad (8)$$

where A and B are the intercept and slope, respectively, which can be calculated using an empirical formula of simple linear regression, and RB (relative backscatter) is the measured backscatter corrected from transmission losses (units are dB) [42].

After gaining the value of SSC during the passage of bores, the instantaneous suspended sediment flux per unit area was quantified based on the value of SSC and the longitudinal turbulent velocity (V_x) [27] as follows:

$$Q_s = SSC \times V_x \quad (9)$$

where:

Q_s = suspended sediment flux per unit area (kg/m^2/s)
SSC = suspended sediment concentration (kg/m^3)
V_x = longitudinal turbulent velocity (m/s).

3. Results and Discussion

3.1. Tidal Harmonic Analysis in the Kampar River Estuary

Based on tidal harmonic analysis, semidiurnal components are predominant in the Kampar River Estuary with a Formzahl of 0.26 (mixed tide with prevailing semidiurnal). Several scholars also reported that the semidiurnal component significantly controls water mass transfer within estuaries throughout the Malacca Strait [3,25,34]. In the Malacca Strait, the tidal distribution is transformed from semidiurnal to a mixed tide with prevailing semidiurnal from Aceh to Riau Province [33]. Even though the semidiurnal components are predominant, the diurnal constituents could not be neglected, influencing the water level fluctuation within the Malacca Strait.

The tidal harmonics results recorded at station MD-1 were compared with the result of the tidal model (Table 2). Overall, both simulated and observed data showed an agreement in constituent amplitude and phase lag with a deviation (RMSE) of less than 5 cm. This indicates that the tidal simulation result could represent the natural conditions of the study area. Because of the gap in time series between the field and model data, a digression is possible [25]. The amplitude of semidiurnal main components was 3 cm higher than the simulated data. The main diurnal component showed a slight difference (<2 cm).

Table 2. Tidal harmonic analysis in the Kampar River estuary.

Tidal Constituents	Simulated Data		Observed Data		Angular Frequency (Degree/Hour)	RMSE (cm)	Species
	Amplitude (cm)	Phase Lag (°)	Amplitude (cm)	Phase Lag (°)			
M2	113.02	199.25	115.74	164.77	28.98	1.92	Principal lunar semidiurnal
S2	52.78	35.09	55.80	49.92	30.00	2.21	Principal solar semidiurnal
N2	24.87	188.15	29.98	157.23	28.44	3.61	Larger lunar elliptic semidiurnal
K2	11.26	104.60	11.96	191.47	30.08	0.49	Lunisolar semidiurnal
K1	36.61	89.55	34.19	50.56	15.04	1.71	Lunar diurnal
O1	23.36	42.29	27.57	69.69	13.94	2.98	Lunar diurnal
P1	14.40	−54.15	11.92	−45.38	14.96	1.75	Solar diurnal
M4	15.14	−4.08	15.02	−2.41	57.97	0.08	Shallow water over-tides of principal lunar
MS4	13.96	187.41	12.01	170.24	58.98	1.38	Shallow water quarter diurnal

Compared to all analyzed tidal constituents, the principal lunar and solar semidiurnal components (M2 and S2) showed a strong amplitude in the Kampar Estuary (Table 2). According to [40], the co-tidal amplitude could determine the distribution of tidal type, and the phase lag differences could reflect the tidal range cycles. In addition to phase lag, despite a large gap between model and field data with <60° resulting from different data frequencies, the phase lag resulting from tidal harmonic analysis could determine interactions among constituents and reflect the variability of the tidal current [44]. In semidiurnal tidal regimes, the flood or ebb dominance is quantified from the relationship between M2 and M4 phase lags [40]. From the harmonic analysis, we calculated that the value of $2g_{M2} - g_{M4}$ ranged between $-90°$ and 90°. Therefore, the Kampar Estuary is characterized by a more prolonged and intense ebb than flood current (ebb dominant). The flood–ebb phase and duration in the Kampar Estuary will be elucidated in the next section.

Concerning the diurnal constituents, the Kampar River mainstream extent from station KP-3 to KP-4 (approximately 70.16 km) was selected for the tidal analysis with the specified observation points right at the ADCP deployment coordinates (Figure 4). During the time frame of field measurement, the study area was subjected to neither the extreme effect of winds nor large freshwater flows. The extent of semidiurnal constituent amplitude distribution upstream was observed and its influence evoking the free surface elevation extended up to approximately 104 km upstream. Overall, the spatial magnitude of the M2 and S2 components gradually increased upstream. The peak magnitude was observed at station KP-2 (Teluk Meranti), with an amplitude of 1.63 m and 1.05 m for M2 and S2, respectively (Figure 4C,D). The magnitude decreased significantly toward station KP-4 (Tanjung Tersendu-sendu), indicating less tidal influence evoking flood discharge throughout the river. These results show that the tidal bore commenced decaying after passing Teluk Meranti station (KP-2). However, aside from tidal regimes, tidal bore propagation relies on bottom morphology, channel formation, and river discharge [4]. These primary co-tidal constituents (M2 and S2) play a significant role in evoking the tidal range-induced tidal bore characteristics in the estuary of Kampar River.

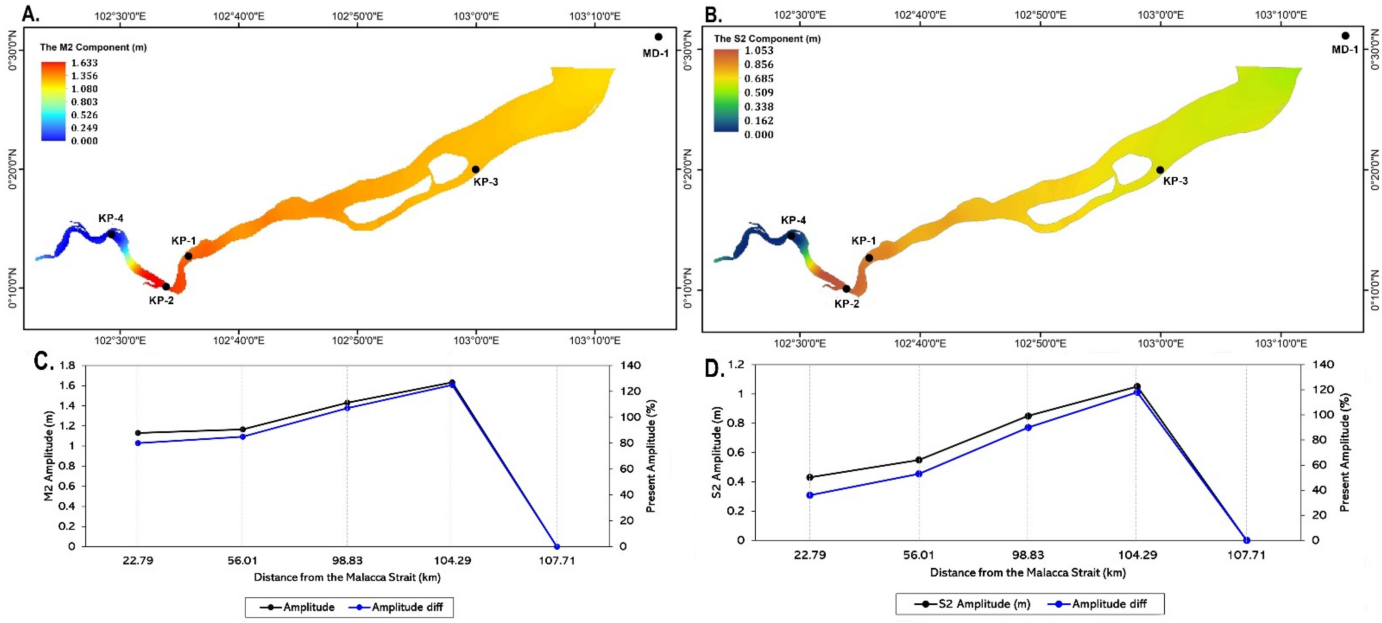

Figure 4. Spatial variability of the dominant tidal component distribution throughout the study area. M2 component distribution (**A**); S2 component distribution (**B**); amplitude and percentage of amplitude difference of M2 (**C**) and S2 (**D**). The amplitude difference percentage computes the amplitude fraction at each station to the amplitude at the mouth of the river (M1).

3.2. Tidal Range Profiles and Tidal Bore Generation

Due to the importance of tidal fluctuation characteristics in the estuary, the minimum range to evoke tidal bore passage has been previously explained (exceeding 4–6 m) [10,26]. The analysis of tidal range and flood–ebb duration is essential to understanding the variability of tidal bore propagation. The process in the estuarine system relies on tidal dynamics related to mixing and sediment transport. Therefore, since the tidal variability depends on the moon phase, the propagation of tidal bores generated in the Kampar Estuary could be distinguished by various astronomical forces. Generally, the tidal range peaked during the full moon phase (spring tidal state) and declined considerably during the third quarter of the moon phase (neap tidal state). However, the flood–ebb displacement duration was longer during neap phases (Figures 5 and 6).

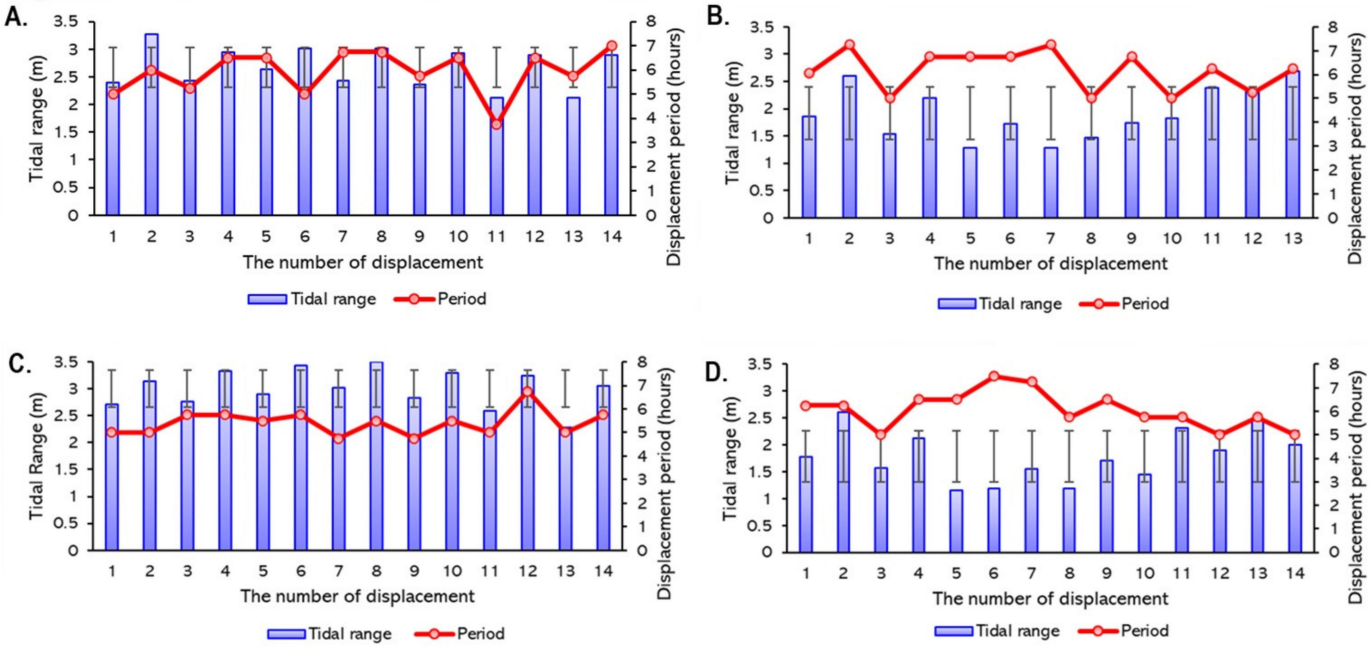

Figure 5. Flood tidal range at the Kampar Estuary during the new moon phase (**A**); during the first quarter of the moon phase (**B**); during the full moon phase (**C**); and during the third quarter of the moon phase (**D**). The grey lines denote the standard deviation.

During the new moon phase, the tidal range during flood tides ranged from 2.3 to 3.3 m, with a flood duration ranging from 4 to 7 h (Figure 5A). The magnitude decreased by around one meter, with a longer flood duration (on average 6 h) during the first quarter of the moon phase (Figure 5B). The highest elevation was observed during the full moon phase, ranging from 2.2 to 3.5 m, with a mean flood duration of 5.5 h (Figure 5C). The remnant phase showed the lowest range in tidal elevation, ranging from 1.3 to 2.6 m, with a flood duration of approximately 6 h (Figure 5D).

A more significant range was observed during ebb tides compared to the flood tides (Figure 6). The tidal range ranged from 2 to 3.7 m with an average ebb duration of 6.5 h during the new moon phase. The tidal range declined significantly during the first quarter of the moon phase, where the ebb-tidal range ranged from 0.9 to 3 m, and the ebb displacement duration ranged from 5 to 8 h. During the full moon phase, the more extreme ebb tides peaked at more than 4 m in the tidal range, with a longer ebb duration of approximately 7 h. In contrast, the lowest range was observed during the third quarter of the moon phase, with a tidal range of 0.5–3 m and an ebb duration of 6.5 h.

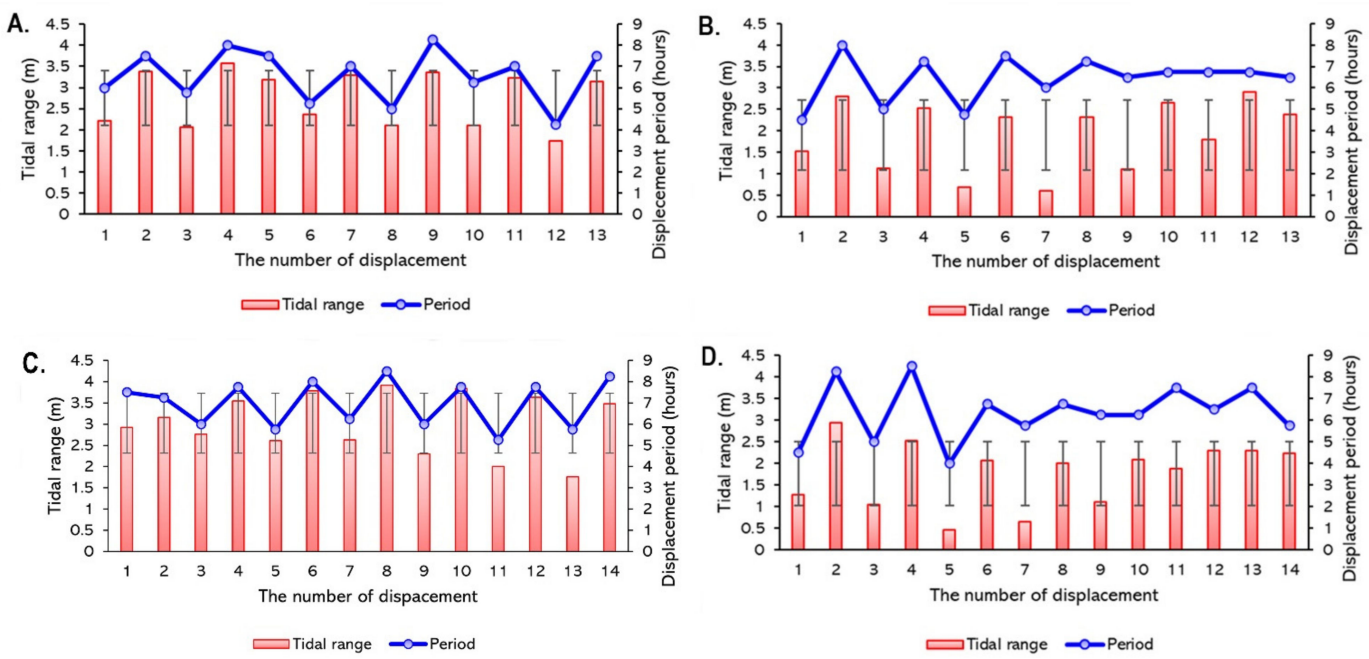

Figure 6. Ebb tidal range at the Kampar Estuary during the new moon phase (**A**); during the first quarter of the moon phase (**B**); during the full moon phase (**C**); and during the third quarter of the moon phase (**D**). The grey lines denote the standard deviation.

Generally, spring tidal states for both the new moon and full moon phases (spring tidal condition) showed a higher tidal range than the moon quarter phases (neap tidal condition). By contrast, the displacement duration was longer during the moon's quarter phases, although the deviation was not too significant. According to [45], the full moon phase evokes the highest sinusoidal tidal level, where the tidal range would be significant during the spring tidal phase. Concerning the tidal range-induced tidal bore propagation, the higher magnitude of the tidal range parameter synchronized with a higher river discharge would induce a higher tidal bore height with a more robust turbulent velocity [7,26]. This aspect is addressed in Section 3.3.

In addition to the ebb dominance of Kampar Estuary, the previously discussed results are in accordance with the tidal phase lag analysis. This condition may vary and be different in the other estuaries throughout the eastern coast of Sumatra due to the difference in latitude-induced co-tidal characteristics [44]. Therefore, examining the characteristics of tidal currents in all estuaries throughout the east coast of Sumatra for further studies is necessary to understand the variation in tidal-induced water motion in the estuarine area.

3.3. Hydraulic Jump Properties of Tidal Bores

A hydraulic jump off a tidal bore is marked by a sudden transition in velocity in rivers or canals where the robust velocity deforms to be a slower motion followed by a sudden rise in free-surface elevation [2,11]. Moreover, the hydraulic jump can be observed from the tidal bore front when rapid changes in water level and velocity take place. Based on the ADCP measurement, we displayed the record of hydraulic jumps at the four observation stations (stations KP-1 to KP-4). Of particular concern, the tidal bore height declined by approximately 1.5 m every 20 km upstream with a non-uniform pattern of turbulent velocity in every observation station (Figure 7). It is expected that the morphology and channel formation play a significant role in determining the variability of the turbulent velocity throughout the Kampar Estuary.

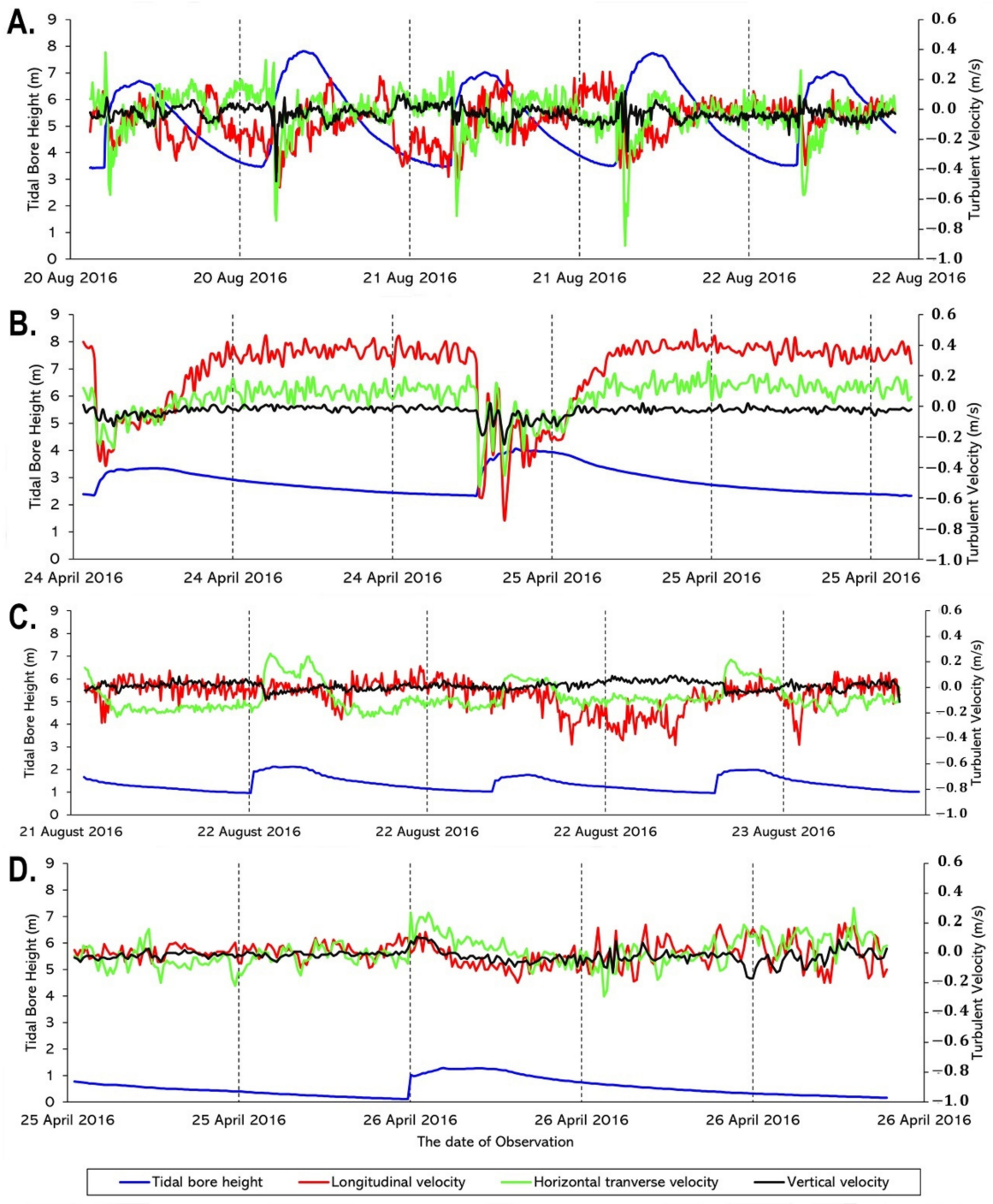

Figure 7. Hydraulic jump properties of tidal bores at station KP-3 (Baru Island) (**A**), KP-1 (Tanjung Tersendu-sendu) (**B**), KP-2 (Teluk Meranti (**C**), and KP-4 (Tanjung Mentangor) (**D**).

At station KP-3 (Baru Island), the water elevation altered from about 3.5 m to 6.8 m and 8 m during tidal bore passage at midday and night, respectively (Figure 7a). Therefore, the tidal bore height in this station was 3.3 m during midday propagation and 4.5 m during night propagation. Before the train of bores passed through the station, a rapid transitional change in turbulent velocity was observed. The longitudinal velocity V_x was negatively upstream, ranging from 0 to -0.4 m/s and positively downstream, ranging from 0 to 0.2 m/s. Its sharp increase in magnitude occurred at the end of the ebb tide, with approximately 0.6 m/s upstream. The longitudinal velocity profile was not significantly different between midday and night passages of bores even though the free surface level was 1.5 m different

in magnitude. Moreover, the negative value of longitudinal velocity detected while the bores were passing by indicates the flow reversal within the channel [26,46].

Unlike the longitudinal velocity, a sudden increase in transverse velocity was observed after the train of bores passed the station. A sharp increase was detected simultaneously with the peak phase of the tidal bore (reaching −0.9 m/s during night propagation). Since the V_y was negative to the river shoreline and positive to the nearby island [5], the sufficiently high negative value indicates the potential of shoreline erosion in the Baru Island. This consideration was proven by [29] based on Landsat records from 1990 to 2007, where significant erosion had occurred in Baru Island with an average change of 2.48 m and a rate of 0.15 m/year. On the other hand, we found that the upward vertical velocity V_z, ranging from −0.4 to 0.1 m/s, significantly evoked a downward movement at the time of the peak surface level during night passages with respect to the theory of a recirculation bubble (turbulence) beneath the first wave crest, as previously explained [1] (see Figure 3).

At station KP-1 (Tanjung Tersendu-sendu), the tidal bore height ranged from 1 to 1.5 m with 2.5 m water depth prior to the passage of bores (Figure 7B). Unlike the KP-3 station, the positive longitudinal velocity was higher by about 0.2 m/s, indicating the ebb stream flow was significant in this area. The reversal flow of the tidal bore was marked by a sudden decrease in longitudinal velocity of about 0.6 m/s negative upstream. The pattern of horizontal transverse velocity tended to be as stable as the previous station, ranging from −0.4 to 0.2 m/s. In this station, an indication of erosion was not expected because no sharp decrease in transverse velocity was detected. Moreover, the variability of turbulent velocity was significant during the night passage of bores. The vertical velocity was not too significant, ranging from 0 to −0.2 m/s at the end of the ebb tides (Figure 7B).

The following observation station (station KP-2) is located 6.26 km from station KP-1. The surface-level change was not too significant, approximately 1 m at both night and midday propagation (Figure 7C). This area is super shallow, with a water depth at the end of the ebb tide of about 1 m, and while the bores were passing this station, the water depth increased by 1 m. The feature of turbulent velocity did not reflect the characteristics of hydraulic jump, where the transverse horizontal velocity showed a particular positive pattern during the passage of bores, indicating that the main flow rotates toward the Teluk Meranti shoreline. The longitudinal velocity was shallow, below 0.2 m/s at the end of the ebb tide, and it slightly decreased by −0.4 m/s while the bores propagated, although this pattern was not applicable for all flood flows. In contrast, the opposite pattern of the horizontal transverse velocity feature was identified where its value was positive during the passage of bores, indicating the water motion flowed toward the northern river shoreline, whereas the vertical velocity showed a small magnitude, ranging from 0.1 to −0.1 m/s (Figure 7C).

The remnant station is KP-4 (Tanjung Mentangor). This station was shallower than KP-2, where the water depth at the end of the ebb tide was close to 0 m. This state was also proven by the presence of sandbanks surrounding this station. The tidal bore height was not too significant (<1 m), indicating a decayed area of tidal bore propagation [20]. No more sharp increases in turbulent velocity were observed in this area ranging from −0.1 to 0.1 m/s.

Overall, the turbulent velocity and water level change properties are consistent with the earlier field study in other bore-affected estuaries [2,7,25,26,47]. As elucidated beforehand, the turbulent velocity profiles, particularly the horizontal transverse circulation, are possibly linked with the irregular channel cross-section and the evolution of the estuary. In this study, the record of hydraulic jump properties is very limited. Therefore, a long-term measurement is recommended to monitor the variability of tidal bore features, which is imperative for future decision-making and development.

The turbulent velocity regime may control sediment transport throughout the river. A previous study determined that the variability of transverse and vertical velocity affecting the secondary currents behind the bore front plays a significant role in evoking sediment resuspension advected upstream [26]. This transport mechanism is linked to

very-strong turbulent mixing determining the erosion and accretion in the upper estuarine zone. Therefore, the fluctuation of suspended sediment beneath the passage of bores is essential to understand.

3.4. Suspended Sediment Concentration and Flux during the Passage of Bores

As the less dynamic tidal bore flow upstream, we displayed the fluctuation of suspended sediment recorded at station KP-3 (Baru Island), whereby the result depicted was measured in the surface bottom layer. The period shown in Figure 8 was sampled during the night passage of the bore, when the tidal bore height was more significant. At the end of the ebb tide, the suspended sediment concentration (SSC) ranged from 0.4 to 0.9 kg/m^3. Compared to Landsat OLI imagery surface layer detection [17], a lower SSC in Kampar River was observed ranging from 0.042 to 0.241 kg/m^3 at the end of the ebb tide.

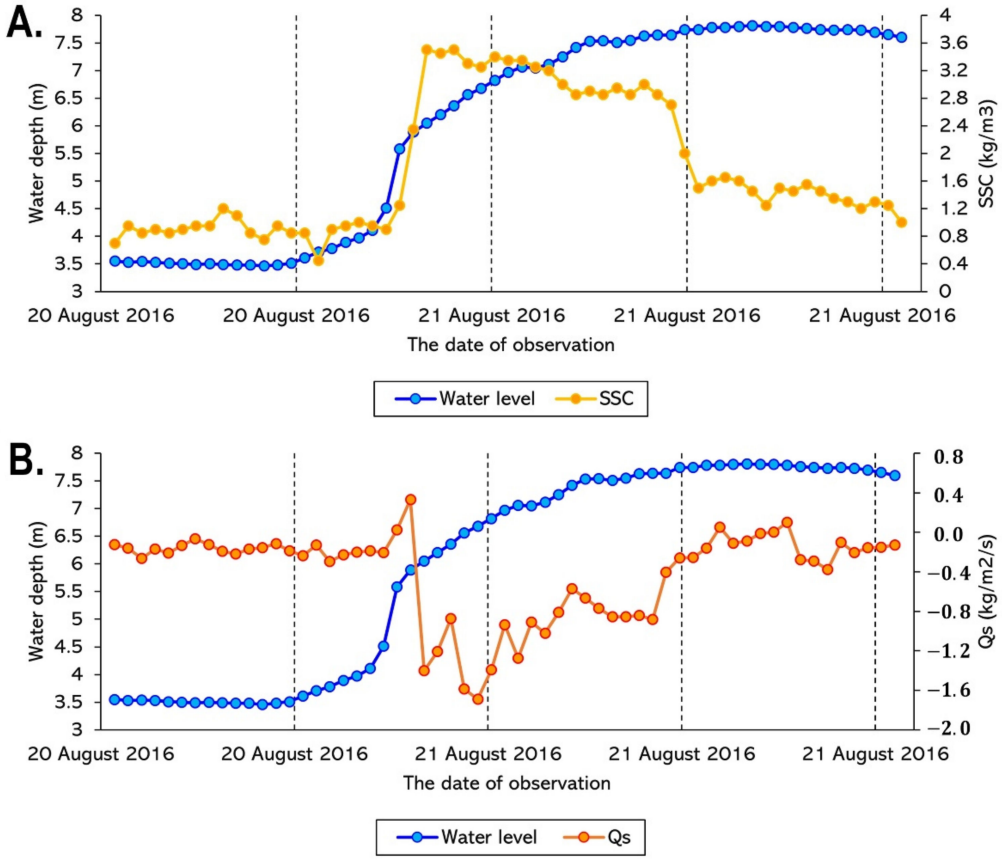

Figure 8. Time series of bore propagation-induced sediment transport at station KP-3. The SSC fluctuation beneath the first wave crest (**A**); the mean sediment flux per unit area (**B**).

When the sudden change in water level occurred, the SSC significantly increased, reaching approximately 3.62 kg/m^3, and it gradually decreased as the bore propagated on average about 2.9 kg/m^3. The peak of SCC occurred beneath the second trough of the tidal bore passage. According to [26], the eroded materials placed in suspension behind the bore front were advected by the "whelps" and secondary current movements. When the water level reached its peak magnitude, it gradually declined, followed by a gradual decrease of SSC in the surface bottom ranging from 0.9 to 1.34 kg/m^3 (Figure 8A).

The result of SSC estimation was consistent with the turbulent velocity regimes where the horizontal transverse and vertical velocity showed a sharp increase in magnitude behind the first wave crest, reflecting an overwhelming erosion that occurred on the surface bottom and near the river edge. The suspended materials are brought by the train of bores upstream, and they are deposited in the area of tidal bore decay (station KP-4), proven by the formation of sandbanks in the middle of the river composed of coarse sediments [4].

The instantaneous suspended sediment flux per unit area Q_s data are displayed in Figure 8B. The sediment flux data revealed a downstream positive mass flux at the end of the ebb tide. Before the tidal bore passage, the suspended sediment flux per unit area was an average of -0.2 kg/m^2/s. When the sharp increase in longitudinal velocity magnitude occurred, it induced a sudden increase in the flux of suspended materials, with a deviation of 0.5 kg/m^2/s. As previously defined by [27], an abrupt reversal flow occurred during the flood tide, marking the passage of bores, and the suspended sediment flux was negative. Shortly after the bore passage, the sediment flux per unit area reached its peak magnitude, with negative values ranging from –0.8 to –1.8 kg/m^2/s, indicating a significant fluctuation of sediment flux. About 2 h after the first wave passed by the station, the sediment flux was approximately -0.3 kg/m^2/s.

The sediment flux data were integrated over time to provide the net sediment mass transfer per unit area over a given period [26,27]. Prior to the passage of the tidal bore (23:50 > t > 24:00), the net sediment mass per unit area was transferred approximately +321.6 kg/m^2 within 10 min of the data. Following the tidal bore passage, the net sediment mass transfer equaled -3028.5 kg/m^2 within 25 min (24:00 > t > 00:25). In contrast, at the end of the bore passage before ebb, the net sediment mass transfer equaled -4068.9 kg/m^2 within 90 min (01:30 > t > 03.00) (Figure 8B). Overall, during the passage of bores, the net sediment mass transfer was estimated to be 3.7 times larger in magnitude than at the early flood tide and 2.6 times larger than the net sediment mass transfer magnitude toward the ebb tide. These trends observed in the present study are consistent with several earlier studies that highlighted that the intense sediment mixing, and upstream advection of suspended materials occurred during the passage of bores [26,27,48].

In addition to sedimentary movement, the surface bottom of the river is subjected to significant stress reversals when it receives cyclic loading during the tidal bore resuspending the cohesive sediment underneath the second trough of the tidal bore train. Because the riverbed is saturated, pore pressure changes occur during "rapid cycling," i.e., the pace of cycling is such that pore pressure variations are not dissipated [49]. As a result, the riverbed may liquefy, causing bed materials to be suspended and transported upstream by the bores.

3.5. Implication of the Tidal Bore Passage to the Surrounding Environment

As mentioned previously, the very high magnitude of horizontal transverse and vertical velocity potentially induces local erosion of the surface bottom and the river edge. The indication of river shoreline erosion at station KP-3 is shown in Figure 9A. Due to the dynamic tidal bore passage, the river shoreline gradually changes over time. According to [29], over 16 years (1990–2016), the area prone to abrasion was detected in the surrounding Baru and Muda Island, with the eroded area reaching 2.36 ha/year. The remarkable celerity of the tidal bore was recorded in several river edges (Figure 9B), where the line track of the tidal bore showed the high erosion induced by the significant transverse velocity. According to [26], the tidal bore can cause significant damage to riverbanks, and navigational hazards in tidal bore have affected estuaries.

On the other hand, due to the long wave propagation surging upstream (tidal bore), the Kampar River is well known for its long-distance surfing. Local government and other third parties promote this attraction for enhancing the local tourism [50], where it is reported that the annual festival "Bakudo Bono," meaning riding the tidal bore through surfing techniques, is held in Teluk Meranti, attracting not only domestic but also foreign tourists [51].

Significant river shoreline changes over time threaten local society where tidal flooding occurs at certain times and houses are devastated (Figure 9C). This tragedy also happens in the Qiantang River, where its banks are overtopped by tidal bore, and dozens of local settlements are drowned yearly [26]. Other tragic examples of drownings in tidal bores and "whelps" include multiple human deaths in the Colorado River (Mexico), Bamu and Fly River (PNG), and Seine River (France) [2]. On the other hand, indigenous boats are often

sunk in the middle of the river due to the intense morphological alteration [6,17]. Therefore, a sustainable water level and regular bathymetry survey are crucial to understanding tidal bore behavior better. Moreover, a model-based estimation can also predict extreme phases of the tidal bore in the Kampar River estuary. The local and central governments must initiate these efforts to construct future development and management.

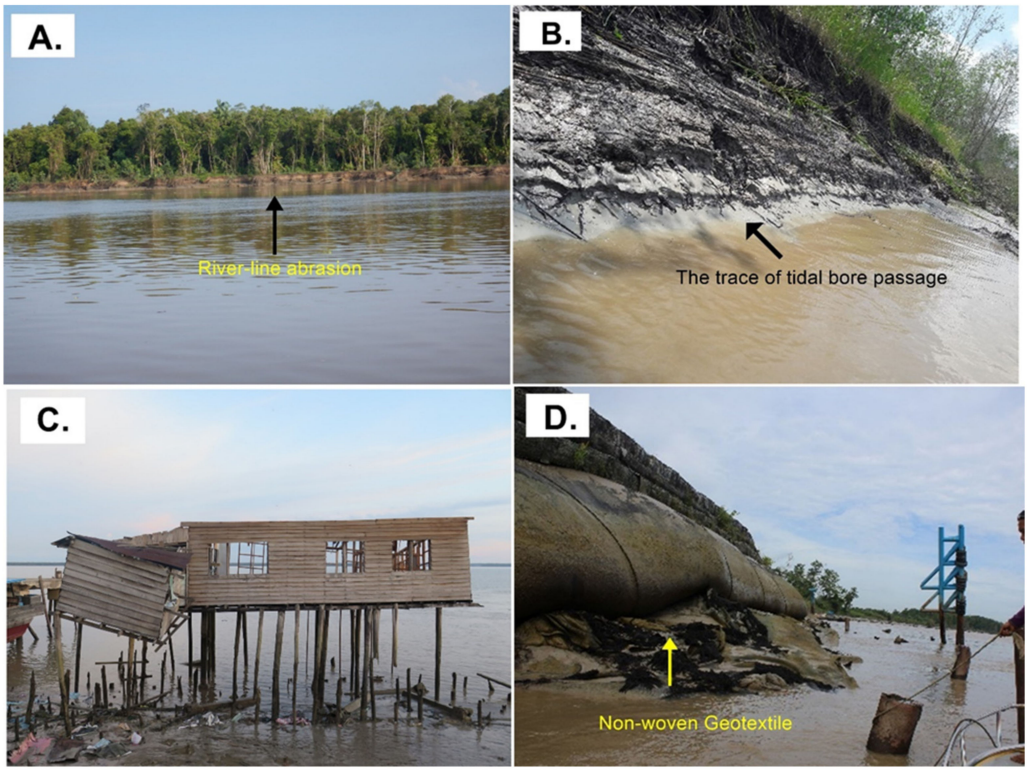

Figure 9. The impact of tidal bore propagation on the surrounding environmental conditions. River-line abrasion (**A**); coastal erosion at the edge of the river (**B**); local settlement destruction due to tidal bore (**C**); non-woven geotextile fabrics as coastal protection applied in several areas of interest (**D**).

The unstable river shoreline changes in the Kampar Estuary previously reported by [29], where a significant river shoreline change was detected from 2010 to 2016 at a rate of 3.56 m/year, may be worsened by some man-made structures constructed in recent years. In several vital areas, particularly the shoreline near the wood-cutting factory, temporary coastal structures were built around the 2000s [52], such as non-woven geotextile container technology (Figure 9D). This kind of structure could significantly protect the river shoreline from destructive waves [53], but on the other hand, the possibility of unstable erosion–sedimentation in the nearby areas due to coastal structures cannot be neglected [4]. As reported by [54], in a coastal area with rapid erosion, declivous slope, and significant waves regimes, a geotextile container could effectively dampen the waves and induce sedimentation behind the structure by around 50 cm within a year. However, other erosion symptoms have also been reported in some nearby areas [54].

Another anthropogenic activity that causes significant river shoreline changes in the Kampar Estuary is sand mining since the propagation of tidal bores relies on bottom morphology. A significant change in bottom morphology due to sand mining activity throughout Kampar River will alter the feature of the tidal bores [4]. As reported by the Department of Energy and Mineral Resources of Pelalawan Regency, the most substantial area of sand mining was identified in Teluk Meranti village, with a total area of 47,701,000 m^2 and sediment volume of 83,400,000 m^3 (Table 3). These results also correlate with the previous report of river shoreline changes [29]. Even though sand mining activity has declined, the practice is still occurring illegally [28]. Therefore, the potency of shoreline erosion due

to tidal bores and anthropogenic activities is still high. Sustainable monitoring of tidal bore properties and sediment dynamics is necessary to control the shoreline instability and minimize other impacts on local society.

Table 3. Record of sand-mining area and volume in 2009 in the Kampar River estuary reported by the Department of Energy and Mineral Resources, Pelalawan Regency [55].

Location	Area (m^2)	Volume (m^3)
Teluk Meranti village	41,701,000	83,400,000
P. Muda village	23,270,000	46,540,000

4. Conclusions

As a semidiurnal-affected water region, water motion throughout the Kampar Estuary is controlled by semidiurnal components (M2 and S2) and their derivatives, characterized by more prolonged and intense ebb than flood currents (ebb dominant). The tidal range during ebb tides is slightly higher, with a longer displacement time than the flood condition. However, spring tidal conditions produce higher elevation (peaking at 4 m) and shorter tidal duration. The amalgamation between the tidal range–duration and the fluctuation of river discharge determines the tidal bore generation.

The tidal bore height declines by approximately 1.5 m every 20 km upstream with an arbitrarily erratic turbulent velocity profile. The rapid increase in horizontal transverse and vertical velocity detected in the estuary determines a strong turbulent mixing affecting the erosion and accretion in the upper estuarine zone (river edge erosion). In the upstream area, the sign of hydraulic jump is not too significant, reflecting the decay phase of the tidal bore indicated by several sandbanks in the middle of the river body, where the suspended sediment deposition is predominant.

The SSC increases significantly by four times in magnitude during the passage of bores and gradually declines as ebb tides occur. In contrast, an abrupt reversal flow occurring during the flood tide induces a negative suspended sediment flux per unit area, where the net sediment mass transfer is estimated to be 3.7 times larger in magnitude than at the early flood tide and 2.6 times larger than the net sediment mass transfer magnitude toward the ebb tide. The properties of suspended sediment induced by the hydraulic jump off a tidal bore play a significant role in the morphodynamical alteration of Kampar Estuary. Therefore, long-term monitoring of tidal bore properties is crucial to support future studies and research-based decision-making regarding further developments in Pelalawan Regency, Riau Province.

Author Contributions: Conceptualization, U.J.W., Y.J.W. and Y.H.; methodology, U.J.W., Y.J.W. and Y.H.; software, U.J.W.; visualization, U.J.W.; validation, U.J.W. and Y.J.W.; formal analysis, U.J.W.; resources, U.J.W.; writing—original draft preparation, U.J.W.; writing—review and editing, U.J.W. and Y.J.W.; supervision, Y.J.W. and Y.H.; funding acquisition, Y.H. All authors have read and agreed to the published version of the manuscript.

Funding: This study was financially supported by a Grant-Aid for Scientific Research (C-2) from the Ministry of Education, Culture, Sports, Science, and Technology of Japan (20K04708).

Institutional Review Board Statement: Not applicable.

Informed Consent Statement: Not applicable.

Data Availability Statement: The data used during the study appear in the submitted article. All secondary data for this paper are cited and referred to in the reference list. Tidal prediction data can be retrieved from a webpage: https://srgi.big.go.id/tides currently accessed on 12 August 2022.

Acknowledgments: We would like to thank the Research Institute for Coastal Resources and Vulnerability, Ministry of Marine Affairs and Fisheries of Indonesia for supporting the observational data used in this study, Ing. Semeidi Husrin, and Wisnu A. Gemilang for the constructive advice

regarding theoretical and conceptual aspects of a tidal bore. Gratitude is also given to Department of Physics and Earth Sciences, University of the Ryukyus and MEXT Scholarship.

Conflicts of Interest: The authors declare no conflict of interest.

References

1. Li, Y.; Pan, D.Z.; Chanson, H.; Pan, C.H. Real-time characteristics of tidal bore propagation in the Qiantang River Estuary, China, recorded by marine radar. *Cont. Shelf Res.* **2019**, *180*, 48–58. [CrossRef]
2. Chanson, H. Environmental, Ecological, and cultural Impacts of Tidal Bores, Burros and Bonos. In Proceeding of the International Workshop on Environmental Hydraulics; Theoretical, Experimental, and Computational Solutions (IWEH), Valencia, Spain, 29–30 October 2009. [CrossRef]
3. Kurniawan, A.; Wisha, U.J.; Husrin, S.; Karjadi, E.A. Tidal Bore Generation at the Estuaries of the East Coast of Sumatra. In Proceedings of the 37th IAHR World Congress, Kuala Lumpur, Malaysia, 13–18 August 2017.
4. Gemilang, W.A.; Wisha, U.J.; Rahmawan, G.A. Particle size characteristics of riverbed sediments transported by tidal bore 'BONO' in Kampar Estuary, Riau-Indonesia. *Mar. Res. Indones.* **2018**, *43*, 25–35. [CrossRef]
5. Chanson, H. Current knowledge in hydraulic jumps and related phenomena: A survey of experimental results. *Eur. J. Mech. B Fluids* **2009**, *28*, 191–210. [CrossRef]
6. Bayu, A.C.; Pudjaprasetya, S.R.; Wisha, U.J.; Husrin, S. Numerical simulation of tidal bore Bono at Kampar River. *J. Appl. Fluid Mech.* **2019**, *12*, 311–318. [CrossRef]
7. Wolanski, E.; Williams, D.; Spagnol, S.; Chanson, H. Undular tidal bore dynamics in the Daly Estuary, Northern Australia. *Estuar. Coast. Shelf Sci.* **2004**, *60*, 629–636. [CrossRef]
8. Docherty, N.J.; Chanson, H. Physical Modeling of Unsteady Turbulence in Breaking Tidal Bores. *J. Hydraul. Eng.* **2012**, *138*, 412–419. [CrossRef]
9. Peregrine, D.H. Calculations of the development of an undular bore. *J. Fluid Mech.* **1966**, *25*, 321–330. [CrossRef]
10. Chanson, H. Mixing and dispersion in tidal bores: A review. In Proceeding of the International Conference on Estuaries and Coasts ICEC, Hangzhou, China, 9–11 November 2003.
11. Chanson, H. *Tidal Bores, Aegir, Eagre, Mascaret, Pororoca: Theory and Observation*; World Scientific: Singapore, 2011; pp. 1–220. [CrossRef]
12. Yulistiyanto, B. The phenomenon of bono rising wave in the Kampar River estuary. *Din. Tek. Sipil* **2009**, *9*, 19–26. (In Indonesian)
13. Rahmawan, G.A.; Wisha, U.J.; Husrin, S.; Ilham, I. Bathymetry and tidal analyses in the estuary of Kampar River: The generation of tidal wave "Undular Bore Bono". *J. Ilm. Geomatika* **2017**, *22*, 57–64. [CrossRef]
14. Asiah, N.; Sukendi, S.; Harjoyudanto, Y.; Junianto, J.; Yustiati, A. Water Quality Analysis Based on Plankton Community Structure in Kampar River, Riau Province. In Proceeding of the IOP Conference Series: Earth and Environmental Science, the 9th International and National Seminar on Fisheries and Marine Science, Pekanbaru, Indonesia, 10–11 September 2020. [CrossRef]
15. Harjoyudanto, Y.; Rifardi, R.; Windarti, W. Water Quality Analysis Around the Floating Net Cage Culture Activities in the Kampar River, Buluhcina Village, Kampar District. In Proceeding of the IOP Conference Series: Earth and Environmental Science, the 8th International and National Seminar on Fisheries and Marine Science, Pekanbaru, Indonesia, 12 September 2019. [CrossRef]
16. Mubarak; Sulaiman, A.; Efriyeldi. Environmental Effect of Tidal Bore Propagation in Kampar River. In Proceeding of the MATEC Web of Conferences, the International Symposium on Civil and Environmental Engineering, Melaka, Malaysia, 5–6 December 2016. [CrossRef]
17. Wisha, U.J.; Dhiauddin, R.; Kusumah, G. Remote estimation of total suspended solid (TSS) transport affected by tidal bore "BONO" of Kampar Big River estuary using Landsat 8 OLI imagery. *Mar. Res. Indones.* **2017**, *42*, 37–45. [CrossRef]
18. Wisha, U.J.; Maslukah, L. Nutrient condition of Kampar Big River estuary: Distribution of N and P concentrations drifted by tidal bore "Bono". *Indones. J. Mar. Sci.* **2017**, *22*, 37–45. [CrossRef]
19. Abdullah, F.A.R.; Ningsih, N.S.; Rachmayani, R. Numerical simulation of tidal bore in Kampar River: A preliminary study. In Proceeding of the IOP Conference Series: Earth and Environmental Science, the first Maluku International Conference on Marine Science and Technology, Ambon, Indonesia, 24–26 October 2018. [CrossRef]
20. Mubarak. Modeling of Kampar River discharge as a solitary wave. *Inter. J. Eng. Technol. UAE* **2018**, *7*, 138. [CrossRef]
21. Putra, Y.S.; Noviani, E.; Nurhasanah; Nurhanisa, M.; Azwar, A. A numerical study of Hydro-Hydraulic energy on Undular Tidal Bore phenomenon. In Proceeding of the Journal of Physics: Conference Series, The 10th International Conference on Theoretical and Applied Physics, Mataram, Indonesia, 20–22 November 2020. [CrossRef]
22. Chanson, H. Momentum considerations in hydraulic jumps and bores. *J. Irrig. Drain. Eng.* **2012**, *138*, 382–385. [CrossRef]
23. Leng, X.; Chanson, H. Coupling between free-surface fluctuations, velocity fluctuations and turbulent Reynolds stresses during the upstream propagation of positive surges, bores and compression waves. *Environ. Fluid Mech.* **2016**, *16*, 695–719. [CrossRef]
24. Madsen, P.A.; Simonsen, H.J.; Pan, C.H. Numerical simulation of tidal bores and hydraulic jumps. *Coast. Eng.* **2005**, *52*, 409–433. [CrossRef]
25. Wisha, U.J.; Wijaya, Y.J.; Hisaki, Y. Tidal bore generation and transport mechanism in the Rokan River Estuary, Indonesia: Hydro-oceanographic perspectives. *Reg. Stud. Mar. Sci.* **2022**, *52*, 102309. [CrossRef]

26. Chanson, H. Current knowledge in tidal bores and their environmental, ecological and cultural impacts. *Environ. Fluid Mech.* **2011**, *11*, 77–98. [CrossRef]
27. Keevil, C.E.; Chanson, H.; Reungoat, D. Fluid flow and sediment entrainment in the Garonne River bore and tidal bore collision. *Earth Surf. Process. Landf.* **2015**, *40*, 1574–1586. [CrossRef]
28. Wisha, U.J.; Rahmawan, G.A.; Ilham, I. *Bono Kuala Kampar, Primadona di Timur Sumatera Yang Terancam Hilang*, 1st ed.; AMAFRAD Press: Jakarta, Indonesia, 2018; pp. 1–89. (In Indonesian)
29. Putra, A.; Wisha, U.J.; Kusumah, G. Spatial analysis of the river line and land cover changes in the Kampar River estuary: The influence of the Bono tidal bore phenomenon. *Forum Geogr.* **2017**, *31*, 220–231. [CrossRef]
30. Matsumoto, K.; Takanezawa, T.; Ooe, M. Ocean tide models developed by assimilating TOPEX/POSEIDON altimeter data into hydrodynamical model: A global model and a regional model around Japan. *J. Oceanogr.* **2000**, *56*, 567–581. [CrossRef]
31. Pratama, M.B. Tidal Flood in Pekalongan: Utilizing and Operating Open Resources for Modelling. In Proceeding of the IOP Conference Series: Materials Science and Engineering, International Conference on Science and Engineering, Gowa, Indonesia, 24 October 2018. [CrossRef]
32. Zainuri, M.; Helmi, M.; Griselda, M.; Novita, A.; Kusumaningrum, H.P.; Koch, M. Improved performance of geospatial model to access the tidal flood impact on land use by evaluating sea level rise and land subsidence Parameters. *J. Ecol. Eng.* **2022**, *23*, 1–11. [CrossRef]
33. Rizal, S.; Damm, P.; Wahid, M.A.; Sündermann, J.; Ilhamsyah, Y.; Iskandar, T.; Muhammad. General circulation in the Malacca Strait and Andaman Sea: A numerical model study. *Am. J. Environ. Sci.* **2012**, *8*, 479–488. [CrossRef]
34. Setiawan, I.; Rizal, S.; Haditiar, Y.; Ilhamsyah, Y.; Purnawan, S.; Irham, M.; Yuni, S.M. Study of current circulation in the Northern Waters of Aceh. In Proceeding of the IOP Conference Series: Earth and Environmental Science, the 2nd International Conference on Marine Science; Better Insight for the Healthy Ocean, Bogor, Indonesia, 6–7 September 2017. [CrossRef]
35. Wyrtki, K. *Physical Oceanography of the Southeast Asian Waters: Scientific Results of Marine Investigations of the South China Sea and the Gulf of Thailand*, 2nd ed.; Scripps Institution of Oceanography, University of California: La Jolla, CA, USA, 1961; pp. 1–195.
36. Chawla, A.; Jay, D.A.; Baptista, A.M.; Wilkin, M.; Seaton, C. Seasonal variability, and estuary-shelf interactions in circulation dynamics of a river-dominated estuary. *Estuaries Coast.* **2008**, *31*, 269–288. [CrossRef]
37. Segeth, K. Some splines produced by smooth interpolation. *Appl. Math. Comput.* **2018**, *319*, 387–394. [CrossRef]
38. Dias, J.M.; Lopes, J.F.; Dekeyser, I. Tidal propagation in Ria de Aveiro lagoon, Portugal. *Phys. Chem. Earth Part B Hydrol. Ocean. Atmos.* **2000**, *25*, 369–374. [CrossRef]
39. Menéndez, M.; Woodworth, P.L. Changes in extreme high water levels based on a quasi-global tide-gauge data set. *J. Geophys. Res. Ocean.* **2010**, *115*, 1–15. [CrossRef]
40. Khojasteh, D.; Chen, S.; Felder, S.; Heimhuber, V.; Glamore, W. Estuarine tidal range dynamics under rising sea levels. *PLoS ONE* **2021**, *16*, e0257538. [CrossRef]
41. Baranya, S.; Józsa, J. Estimation of suspended sediment concentrations with ADCP in danube river. *J. Hydrolog. Hydromech.* **2013**, *61*, 232–240. [CrossRef]
42. Dwinovantyo, A.; Manik, H.M.; Prartono, T.; Susilohadi; Ilahude, D. Estimation of Suspended Sediment Concentration from Acoustic Doppler Current Profiler (ADCP) Instrument: A Case Study of Lembeh Strait, North Sulawesi. In Proceeding of the IOP Conference Series: Earth and Environmental Science, The 3rd International Symposium on LAPAN-IPB Satellite for Food Security and Environmental Monitoring, Bogor, Indonesia, 25–26 October 2016. [CrossRef]
43. Venditti, J.G.; Church, M.; Attard, M.E.; Haught, D. Use of ADCPs for suspended sediment transport monitoring: An empirical approach. *Water Resour. Res.* **2016**, *52*, 2715–2736. [CrossRef]
44. Mao, Q.; Shi, P.; Yin, K.; Gan, J.; Qi, Y. Tides and tidal currents in the Pearl River Estuary. *Continent. Shelf Res.* **2004**, *24*, 1797–1808. [CrossRef]
45. Kvale, E.P. The origin of neap-spring tidal cycles. *Mar. Geol.* **2006**, *235*, 5–18. [CrossRef]
46. Trevethan, M.; Chanson, H.; Takeuchi, M. Continuous high-frequency turbulence and suspended sediment concentration measurements in an upper estuary. *Estuar. Coast. Shelf Sci.* **2007**, *73*, 341–350. [CrossRef]
47. Simpson, J.H.; Fisher, N.R.; Wiles, P. Reynolds stress and TKE production in an estuary with a tidal bore. *Estuar. Coast. Shelf Sci.* **2004**, *60*, 619–627. [CrossRef]
48. Furgerot, L.; Mouazé, D.; Tessier, B.; Perez, L.; Haquin, S.; Weill, P.; Crave, A. Sediment transport induced by tidal bores. An estimation from suspended matter measurements in the Sée River (Mont-Saint-Michel Bay, northwestern France). *Comptes Rendus Géosci.* **2016**, *348*, 432–441. [CrossRef]
49. Donnelly, C.; Chanson, H. Environmental impact of undular tidal bores in tropical rivers. *Environ. Fluid Mech.* **2005**, *5*, 481–494. [CrossRef]
50. Rianto, S.; Santri, S. Obstacles and efforts to develop Bono tourism object in the Kampar River, Teluk Meranti Sub-District, Pelalawan Regency. *J. Spasial.* **2017**, *3*, 71–81. (In Indonesian) [CrossRef]
51. Hidir, A.; Asriwandari, H.; Kartikowati, S.R. Development Strategy for Coastal Society Based on the Development of Bono Tourism (Tidal Bore) in the Pelalawan Regency. In Proceeding of the National Seminar of Politic Bureaucracy, and Social Change in Efforts to Develop National Characters, Pekanbaru, Indonesia, 21 May 2013. (In Indonesian).

52. Persoalan Lahan Masyarakat Rantau Kasih vs. Perusahaan Kayu, Ada Penyelesaian? Available online: https://www.mongabay.co.id/2021/09/15/persoalan-lahan-masyarakat-rantau-kasih-vs-perusahaan-kayu-ada-penyelesaian/ (accessed on 14 August 2022). (In Indonesian).
53. Saathoff, F.; Oumeraci, H.; Restall, S. Australian and German experiences on the use of geotextile containers. *Geotext. Geomembr.* **2007**, *25*, 251–263. [CrossRef]
54. Mahabror, D.; Indriasari, V.Y.; Sofyan, A.; Nugroho, D.; Akhwady, R. Prototype engineering technology of elongated geotextile container as an alternative construction for mitigating abrasion in Pademawu Beach, Pamekasan Regency. *Naturalis* **2021**, *10*, 32–45. (In Indonesian) [CrossRef]
55. Anonymous. *Final Report of Natural Resources Inventory in the Pelalawan Regency 2009*; Department of Energy and Mineral Resources: Pekanbaru, Indonesia, 2009; pp. 221–308. (In Indonesian)